Markov chain models of coupled calcium channels: K

Hilary DeRemigio[1], M. Drew LaM

[1] Dept. of Math. Sciences, U.S. Military A

[2] Dept. of Applied & Computer Science, Colle

— Abstract —

Mathematical models of calcium release sites derived from Markov chain models of intracellular calcium channels exhibit collective gating reminiscent of the experimentally observed phenomenon of stochastic calcium excitability (i.e., calcium puffs and sparks). We present a Kronecker structured representation using stochastic automata networks for calcium release site models and perform benchmark stationary distribution calculations using both exact and approximate iterative numerical solution techniques that leverage this structure. We find multi-level methods provide excellent convergence with modest additional memory requirements. When an exact solution is not feasible, iterative approximate methods based on the power method may be used, with performance similar to Monte Carlo estimates.

— Calcium Release Sites: Puffs and Sparks —

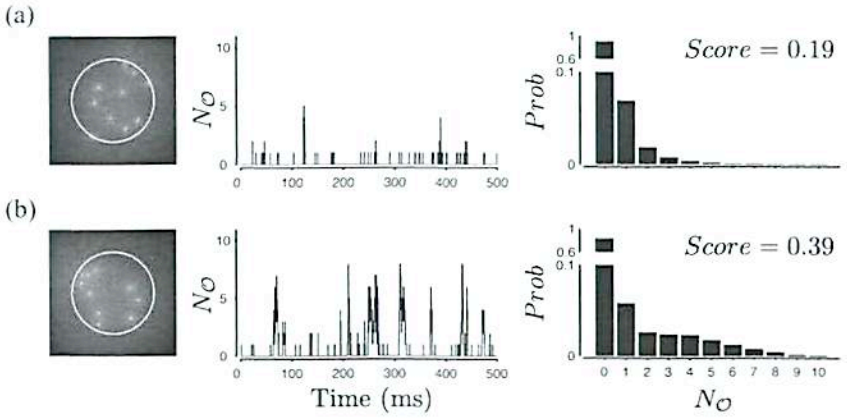

Figure 1: **(a)** Left: $[Ca^{2+}]$ near 3×3 μm endoplasmic reticulum membrane with 12 Ca^{2+}-regulated Ca^{2+} channels modeled as 3-state Markov chains (see Fig. 2(a)) with positions randomly chosen from a uniform distribution on a disc of radius 2 μm (source amplitude 0.05 pA). Buffered Ca^{2+} diffusion is modeled as in [2]. Middle: Stochastic dynamics of the number of open channels at the release site (N_O) that does not include robust puffs/sparks. Right: Probability distribution of the number of open channels leading to a low puff/spark *Score* (see Eq. 2) of 0.19. **(b)** Different random channel positions result in a release site that exhibits robust Ca^{2+} puff/sparks (middle) and an elevated *Score* of 0.39 (right).

— Exact Method

Solver	Max Res
JOR	9.49E-13
JOR_AD	9.44E-13
ARNOLDI	2.42E-13
BICGSTAB	8.66E-13
PRE_ARNOLDI	8.62E-15
BSOR_BICGSTAB	8.22E-15
ML_JOR_F_DYN	5.87E-13

Table 1: Benchmark calculations for 10 3-state channels compu 8GB RAM solving Eq. 1. Description of solvers [1]: JOR, Jac tion/disaggregation; ARNOLDI, the method of Arnoldi; BICGSTAB, Arnoldi with Neumann pre-conditioning; BSOR_BICGSTAB, the bic conditioning; ML_JOR_F_DYN, multi-level method with JOR smoother

— Exact Methods: S

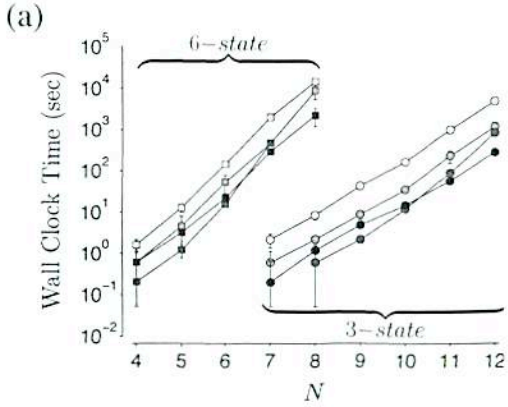

Figure 3: **(a):** *Circles* and error bars show the mean ± SD of wal

ronecker representations and iterative solution methods

ar[2], Peter Kemper[2], Gregory D. Smith[2]

cademy at West Point, West Point, NY, 10996
ge of William and Mary, Williamsburg, VA, 23187

s: Benchmarking —

Sum Res	CPU (s)	Wall (s)	Iters
5.16E-12	279	279	1840
5.13E-12	415	415	1550
4.04E-11	214	215	1440
4.89E-11	146	148	602
1.82E-12	26	27	160
5.29E-13	19	19	52
1.68E-10	15	15	46

ted using Linux PCs with dual core 3.8GHz EM64T Xeon processors and
bi over-relaxation method; JOR_AD, the method of Jacobi with aggrega-
the biconjugate gradient stabilized method; PRE_ARNOLDI, the method of
njugate gradient stability method with block successive over-relaxation pre-
, F cycle, and dynamic ordering.

— Approximate Methods: Partitioning —

$\|\mathcal{P}\|$	Optimal $\mathcal{P}$ for 3-state model	ϵ_π	ϵ_{score}	$\nu(3)$	$\nu(12)$
1	$\{\mathcal{C}_1\mathcal{C}_2\mathcal{O}_1\}$	1.66E+0	9.38E-1	3.33E-1	6.77E-5
2	$\{\mathcal{C}_1\mathcal{C}_2\}\{\mathcal{O}_1\}$	5.40E-3	3.50E-3	1.33E+0	1.39E-1
3	$\{\mathcal{C}_1\}\{\mathcal{C}_2\}\{\mathcal{O}_1\}$	6.00E-8	4.38E-9	3.00E+0	1.20E+1

$\|\mathcal{P}\|$	Optimal $\mathcal{P}$ for 6-state model	ϵ_π	ϵ_{score}	$\nu(3)$	$\nu(8)$
1	$\{\mathcal{C}_1\mathcal{C}_2\mathcal{R}_1\mathcal{R}_2\mathcal{R}_3\mathcal{O}_1\}$	4.84E-1	5.40E-1	8.30E-2	2.86E-5
2	$\{\mathcal{C}_1\mathcal{C}_2\mathcal{R}_1\mathcal{R}_2\mathcal{R}_3\}\{\mathcal{O}_1\}$	3.50E-2	1.36E-2	3.33E-1	3.70E-3
3	$\{\mathcal{C}_1\mathcal{C}_2\}\{\mathcal{R}_1\mathcal{R}_2\mathcal{R}_3\}\{\mathcal{O}_1\}$	7.10E-3	5.50E-3	7.50E-1	6.25E-2
4	$\{\mathcal{C}_1\}\{\mathcal{C}_2\}\{\mathcal{R}_1\mathcal{R}_2\mathcal{R}_3\}\{\mathcal{O}_1\}$	1.90E-4	7.60E-6	1.33E+0	4.68E-1
5	$\{\mathcal{C}_1\}\{\mathcal{C}_2\}\{\mathcal{R}_1\mathcal{R}_2\}\{\mathcal{R}_3\}\{\mathcal{O}_1\}$	5.07E-7	4.12E-8	2.08E+0	2.23E+0
6	$\{\mathcal{C}_1\}\{\mathcal{C}_2\}\{\mathcal{R}_1\}\{\mathcal{R}_2\}\{\mathcal{R}_3\}\{\mathcal{O}_1\}$	4.21E-8	4.16E-8	3.00E+0	8.00E+0

Table 2: Optimal partitioning strategies for APP_POWER listed with their relative errors and memory requirements for both $N = 3$ 3- and 6-state channels with states $\mathcal{S} = \{\mathcal{C}_1, \mathcal{C}_2, \mathcal{O}_1\}$ and $\mathcal{S} = \{\mathcal{C}_1, \mathcal{C}_2, \mathcal{R}_1, \mathcal{R}_2, \mathcal{R}_3, \mathcal{O}_1\}$, respectively (see Fig. 2). The last column also lists relative memory requirements $\nu(N)$ for larger N, where $\nu(N) = Z_A/Z_E$, with $Z_A = NM|\mathcal{P}|^{N-1}$ and $Z_E = M^N$ the memory requirements for the approximate and exact methods, respectively. For the 3-state model, the optimal $\mathcal{P}$ is the best of 1, 3, 1 possibilities when $|\mathcal{P}| = 1, 2, 3$. For the 6-state model, the optimal $\mathcal{P}$ is the best of 1, 31, 90, 65, 15, 1 possibilities when $|\mathcal{P}| = 1, 2, 3, 4, 5, 6$.

Scalability and Error —

(b)

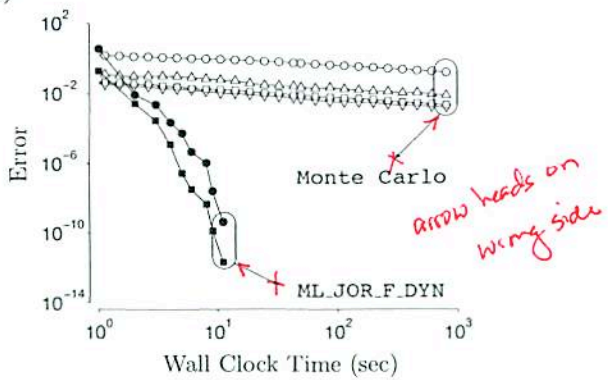

l clock time for five release site configurations of the 3-state model (Fig. 2(a))

— Approximate Methods: Scalability and Error —

(a)

(b)

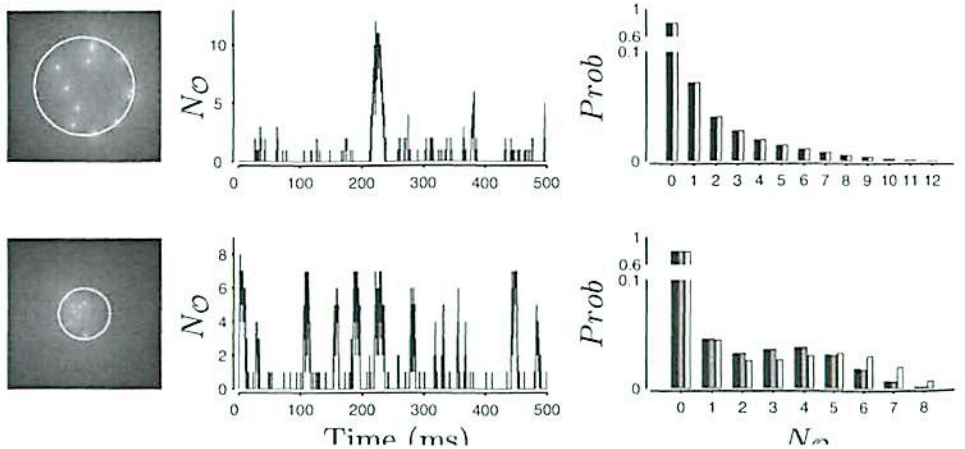

Figure 2: **(a)** 3-state single channel model with Ca^{2+}-mediated activation that has two closed ($\mathcal{C}_1$, $\mathcal{C}_2$) and one open ($\mathcal{O}_1$) state. Parameters in $\mu M^{-1} ms^{-1}$: $k_a^+ = 1.5$, $k_b^+ = 150$; in ms^{-1}: $k_a^- = 50$, $k_b^- = 1.5$. **(b)** 6-state single channel model with Ca^{2+}-mediated activation and inactivation. Parameters in $\mu M^{-1} ms^{-1}$: $k_a^+ = 1.5$, $k_b^+ = k_d^+ = 0.015$, $k_c^+ = k_e^+ = 300$, $k_f^+ = 3.0$; in ms^{-1}: $k_a^- = 49.5$, $k_b^- = k_d^- = 0.2475$, $k_c^- = k_e^- = 6.0$, $k_f^- = 0.03$.

— Model Setup: Exact Methods —

The generator matrix for a single 3- or 6-state channel model takes the form

$$Q = K_- + (c_\infty I + c_d I_{\mathcal{O}})\, K_+$$

where K_- and K_+ are $M \times M$ matrices that collect the unimolecular (k_i^-) and bimolecular (k_i^+) transition rates, M is the number of states in the single channel model, I is the $M \times M$ identity matrix, $I_{\mathcal{O}} = \text{diag}\,\{e_{\mathcal{O}}\}$, and $e_{\mathcal{O}}$ is an $M \times 1$ vector indicating open states of the single channel model [2]. For example, for the 3-state model of Fig. 2(a) we have

$$K_- = \begin{pmatrix} 0 & 0 & 0 \\ k_a^- & -k_a^- & 0 \\ 0 & k_b^- & -k_b^- \end{pmatrix}, \qquad K_+ = \begin{pmatrix} -k_a^+ & k_a^+ & 0 \\ 0 & -k_b^+ & k_b^+ \\ 0 & 0 & 0 \end{pmatrix}$$

In the case of N channels coupled at the Ca^{2+} release site, the expanded generator matrix—i.e., the SAN descriptor—is given by

$$Q^{(N)} = \bigoplus_{n=1}^{N} X_\infty + \sum_{i,j=1}^{N} \bigotimes_{n=1}^{N} X_{ij}^n \tag{1}$$

where $X_\infty = K_- + c_\infty K_+$ and

$$X_{ij}^n = \begin{cases} I_{\mathcal{O}} & \text{for } i \neq j,\ i = n \\ c_{ij} K_+ & \text{for } i \neq j,\ j = n \\ c_d I_{\mathcal{O}} K_+ & \text{for } i = j = n \\ I & \text{otherwise.} \end{cases}$$

We are interested in calculating both the stationary distribution given by

$$\boldsymbol{\pi}^{(N)} Q^{(N)} = \mathbf{0} \quad \text{subject to} \quad \boldsymbol{\pi}^{(N)} e^{(N)} = 1$$

and a coarser measure called the puff/spark *Score* defined as

$$Score = \frac{\text{Var}[f_{\mathcal{O}}]}{\text{E}[f_{\mathcal{O}}]} = \frac{1}{N} \frac{\text{Var}[N_{\mathcal{O}}]}{\text{E}[N_{\mathcal{O}}]}. \tag{2}$$

using: SOR (white), ERE-ARNOLDI (light gray), BSOR-BICGSTAB (d
the 6-state model (Fig. 2(b)). Single-channel parameters as in Fig. 2 C
GB RAM. **(b):** Convergence of response measures for a release site co
and *open* symbols, respectively). *Circles* and *squares* give 1- and ∞-no
puff/spark *Score* for Monte Carlo (mean of 50 simulations shown) cor
the *lower pointing triangles* give the relative error in the probability th

— Model Setup: Ap

For one 3-state channel, the state-space $\mathcal{S}$ with
$\{\mathcal{C}_1, \mathcal{C}_2, \mathcal{O}_1\}$ and $\mathcal{P} = \{\mathcal{C}, \mathcal{O}\}$ with $\mathcal{C} = \{\mathcal{C}_1, \mathcal{C}$
the induced partitioning on the expanded state-s
$s = s^1 s^2 \ldots s^N \in \mathcal{S}^{(N)} \mapsto p = p^1 p^2 \ldots p^N \in$
resentation where the transition matrix Q is dec

$$Q^{(N)}[p,p] = \bigoplus_{n=1}^{N} X_\infty[p^n, p^n] + \sum_{i,j=1}^{N} \mathcal{C}$$

$$Q^{(N)}[p,q] = \left(\bigotimes_{n=1}^{k-1} I_{|p^n|} \right) \otimes X_\infty[p^k, q$$

Compositional representation of π correspondin
The approximate numerical method we consider

— Approximate Method

(a)

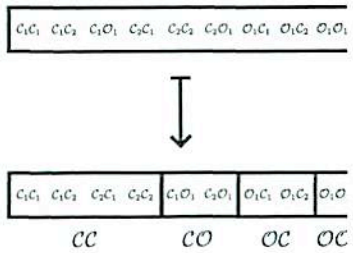

Figure 4: **(a)** Permutation of states and partition structure for N
where $\mathcal{C} = \{\mathcal{C}_1, \mathcal{C}_2\}$ and $\mathcal{O} = \{\mathcal{O}_1\}$. The induced partitioning on $\mathcal{S}^{(2)}$
in both $\mathcal{S}^{(2)}$ and each partition. **(b)** Block structure of the expanded g
denotes the hierarchical structure of the partitioning.

The authors thank Buchholz and Dayar for sharing their implementation of Nsolve. This material is

dark gray), and ML_JOR_F_DYN (*black*). *Squares* and error bars give results for calculations performed using 2.66 GHz Dual-Core Intel Xeon processors and 2 composed of 10 3-state channels using ML_JOR_F_DYN and Monte Carlo (*filled* rms of the residual errors, *upper pointing triangles* give the relative error in the npared with the *Score* given by ML_JOR_F_DYN upon convergence. Similarly, at all N channels are closed. Parameters as in Fig. 1.

pproximate Methods —

n a particular partition structure $\mathcal{P}$ is given by $\mathcal{S} = \mathcal{O}_2\}$, $\mathcal{O} = \{\mathcal{O}_1\}$. In the case of N 3-state channels, pace is a mapping from 3^N states to 2^N partitions by $\mathcal{P}^{(N)}$. We can use the *hierarchical Kronecker rep-* composed into blocks over partitions $p \neq q$ such that

$$\bigotimes_{n=1}^{N} X_{ij}^n[p^n, p^n].$$

$$\left(\bigotimes_{n=k+1}^{N} I_{|p^n|}\right) + \sum_{i,j=1}^{N} \bigotimes_{n=1}^{N} X_{ij}^n[p^n, q^n].$$

to p is $\pi[p] = \alpha_p \bigotimes_{n=1}^{N} \pi_p^n$ with $\sum_{p \in \mathcal{P}^{(N)}} \alpha_p = 1$. that leverages this structure is APP_POWER.

s: Hierarchical Structure —

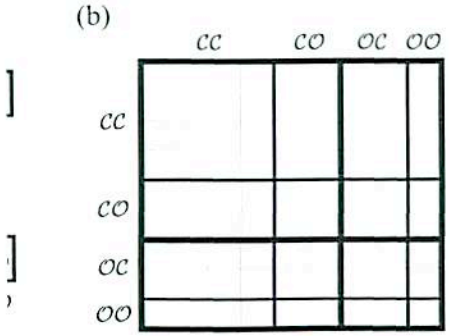

= 2 3-state channels under the closed/open partitioning strategy $\mathcal{P} = \{\mathcal{C}, \mathcal{O}\}$, is thus $\mathcal{P}^{(2)} = \{\mathcal{CC}, \mathcal{CO}, \mathcal{OC}, \mathcal{OO}\}$, with the states ordered lexicographically enerator matrix $Q^{(2)}$ when permuted in this manner. The thickness of the lines

Figure 5: **(a)** Statistics for a release site composed of 12 3-state channels. Left: Local $[Ca^{2+}]$ near $3 \times 3\ \mu m$ ER membrane modeled as in Fig. 1. Middle: Localized Ca^{2+} elevations reminiscent of Ca^{2+} puffs/sparks. Right: Probability distribution of the number of open channels calculated exactly using ML_JOR_F_DYN (*black bars*) and approximately using APP_POWER with $\mathcal{C}/\mathcal{O}$ partitioning (*white bars*). **(b)** Statistics as in A for 8 6-state channels with *black bars* denoting ML_JOR_F_DYN and *white and grey bars* denoting APP_POWER with $\mathcal{C}/\mathcal{O}$ and $\mathcal{C}/\mathcal{R}/\mathcal{O}$ partitioning, respectively.

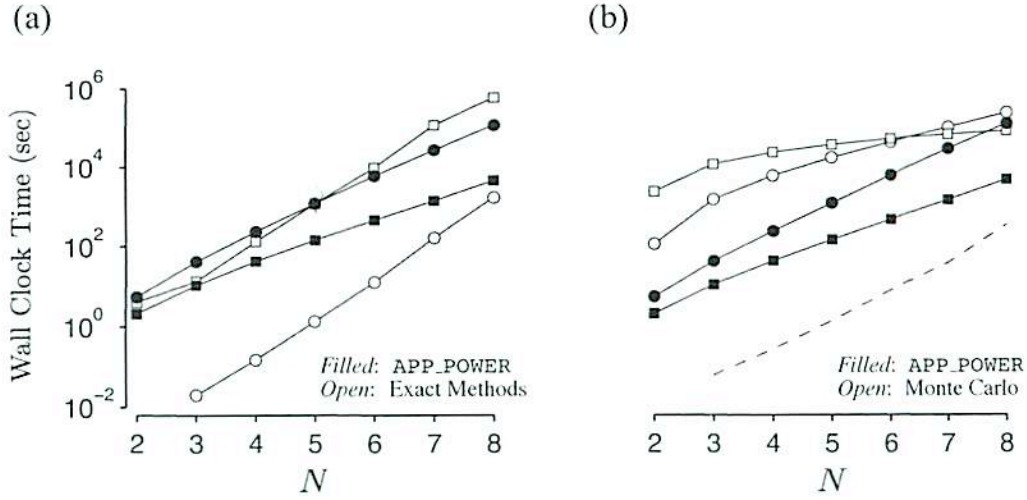

Figure 6: **(a)** *Filled* and *open* symbols show the wall clock time for the 6-state model using approximate and exact methods, respectively. Approximate results are shown for two levels of partitioning ($\mathcal{C}/\mathcal{O}$, *squares* and $\mathcal{C}/\mathcal{R}/\mathcal{O}$, *circles*) with the APP_POWER method. Exact solutions are calculated using the POWER method (*squares*) and ML_JOR_F_DYN method (*circles*). **(b)** Results as in A with *open* symbols corresponding to Monte Carlo estimates of two coarse response measures: the distribution of the number of open channels (*circles*) and the distribution of probability across the M states of an arbitrarily selected individual channel (*squares*). The *dashed line* shows the projected performance of an approximate multi-level solver that uses ML_JOR_F_DYN rather than POWER as its iterative engine.

— References —

[1] W. Stewart, *Introduction to the numerical solution of Markov chains*, Princeton: Princeton University Press (1994).

[2] V. Nguyen, R. Mathias, and G. D. Smith, *A stochastic automata network descriptor for Markov chain models of instantaneously coupled intracellular* Ca^{2+} *channels*, Bulletin of Mathematical Biology, 67 (2005), pp.393–432.

[3] H. DeRemigio, M. D. LaMar, P. Kemper, and G. D. Smith, *Markov chain models of coupled calcium channels: Kronecker representations and iterative solution methods*, Physical Biology, 5 (2008).

based upon work supported by the National Science Foundation under Grants No. 0133132 and 0443843.

Markov chain models of coupled calcium channels: Kronecker representations and iterative solution methods

Hilary DeRemigio[1], M. Drew LaMar[2], Peter Kemper[2], Gregory D. Smith[2]

[1] Dept. of Math. Sciences, U. S. Military Academy at West Point, West Point, NY, 10996

[2] Dept. of Applied & Computer Science, College of William and Mary, Williamsburg, VA, 23187

— Abstract —

Mathematical models of calcium release sites derived from Markov chain models of intracellular calcium channels exhibit collective gating reminiscent of the experimentally observed phenomenon of stochastic calcium excitability (i.e., calcium puffs and sparks). We present a Kronecker structured representation using stochastic automata networks for calcium release site models and perform benchmark stationary distribution calculations using both exact and approximate iterative numerical solution techniques that leverage this structure. We find multi-level methods provide excellent convergence with modest additional memory requirements. When an exact solution is not feasible, iterative approximate methods based on the power method may be used, with performance similar to Monte Carlo estimates.

— Calcium Release Sites: Puffs and Sparks —

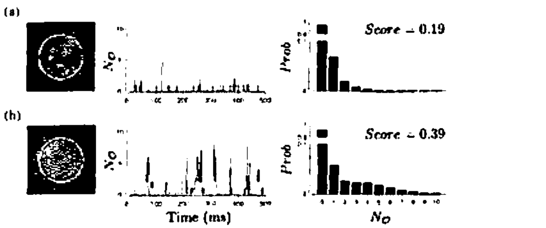

Figure 1 (a) Left: $[Ca^{2+}]$ near [illegible] endoplasmic reticulum membrane with 12 Ca^{2+}-regulated Ca^{2+} channels modeled as 3-state Markov chains (see Fig. 2(a)) with positions randomly chosen from a uniform distribution on a disc of radius 2 [illegible] source amplitude 0.05 pA). Buffered [illegible] diffusion is modeled as in [2]. Middle: Stochastic dynamics of the number of open channels at the release site (N_O) that does not include robust puffs/sparks. Right: Probability distribution of the number of open channels leading to a low puff/spark Score (see Eq. 2) of 0.19. (b) Different random channel positions result in a release site that exhibits robust [illegible] puff/sparks (middle) and an elevated Score of 0.39 (right).

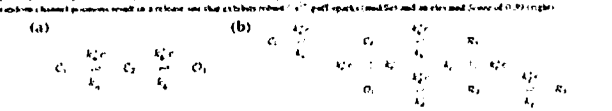

Figure 2 (a) 3-state single channel model with Ca^{2+}-mediated activation that has two closed (C_1, C_2) and one open (O_1) state. [illegible] (b) 6-state single channel model with Ca^{2+}-mediated activation and inactivation. [illegible]

— Model Setup: Exact Methods —

The generator matrix for a single 3- or 6-state channel model takes the form

$$Q = K_- + (c_\infty I + c_d I_O) K_+$$

where K_- and K_+ are $M \times M$ matrices that collect the unimolecular (k_i^-) and bimolecular (k_i^+) transition rates, M is the number of states in the single channel model, I is the $M \times M$ identity matrix, $I_O = \mathrm{diag}\{e_O\}$, and e_O is an $M \times 1$ vector indicating open states of the single channel model [2]. For example, for the 3-state model of Fig. 2(a) we have

$$K_- = \begin{pmatrix} 0 & 0 & 0 \\ k_a^- & -k_a^- & 0 \\ 0 & k_b^- & -k_b^- \end{pmatrix} \qquad K_+ = \begin{pmatrix} -k_a^+ & k_a^+ & 0 \\ 0 & -k_b^+ & k_b^+ \\ 0 & 0 & 0 \end{pmatrix}.$$

In the case of N channels coupled at the Ca^{2+} release site, the expanded generator matrix—i.e., the SAN descriptor—is given by

$$Q^{(N)} = \bigoplus_{n=1}^{N} X_n + \sum_{i,j=1}^{N} \bigotimes_{n=1}^{N} X_{ij}^n \qquad (1)$$

where $X_n = K_- + c_\infty K_+$ and

$$X_{ij}^n = \begin{cases} I_O & \text{for } i \neq j,\ i = n \\ c_{ij} K_+ & \text{for } i \neq j,\ j = n \\ c_d I_O K_+ & \text{for } i = j = n \\ I & \text{otherwise.} \end{cases}$$

We are interested in calculating both the stationary distribution given by

$$\pi^{(N)} Q^{(N)} = 0 \quad \text{subject to} \quad \pi^{(N)} e^{(N)} = 1$$

and a coarser measure called the puff/spark *Score* defined as

$$Score = \frac{\mathrm{Var}[f_O]}{\mathrm{E}[f_O]} = \frac{1}{N} \frac{\mathrm{Var}[N_O]}{\mathrm{E}[N_O]} \qquad (2)$$

— Exact Methods: Benchmarking —

Solver	Max Res	Sum Res	CPU (s)	Wall (s)	Iters
JOR	9.49E-13	5.16E-12	279	279	1040
JOR_AD	9.44E-13	5.13E-12	415	415	1550
ARNOLDI	2.42E-13	4.04E-11	214	215	1440
BICGSTAB	6.44E-13	6.69E-11	144	149	622
PRE_ARNOLDI	8.62E-15	1.92E-12	26	27	159
BSOR_BICGSTAB	6.23E-15	5.29E-13	19	19	52
ML_JOR_F_DYN	5.07E-13	1.68E-10	15	25	65

Table 1 Benchmark calculations for 10 3-state channels computed using Linux PCs with dual core 3.8GHz EM64T Xeon processors and 8GB RAM solving Eq. 1. Description of solvers [1]: JOR, Jacobi over-relaxation method; JOR_AD, the method of Jacobi with aggregation-disaggregation; ARNOLDI, the method of Arnoldi; BICGSTAB, the biconjugate gradient stabilized method; PRE_ARNOLDI, the method of Arnoldi with Neumann pre-conditioning; BSOR_BICGSTAB, the biconjugate gradient stability method with block successive over-relaxation pre-conditioning; ML_JOR_F_DYN, multi-level method with JOR smoother, F cycle, and dynamic ordering.

— Exact Methods: Scalability and Error —

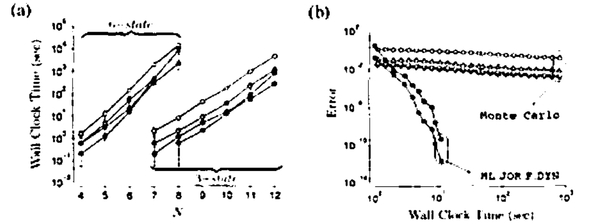

Figure 3 (a) Circles and error bars show the mean ± SD of wall clock time for five release site configurations of the 3-state model (Fig. 2(a)) using JOR (white), PRE_ARNOLDI (light grey), BSOR_BICGSTAB (dark grey) and ML_JOR_F_DYN (black). Square and error bars give results for the 6-state model (Fig. 2(b)). Single channel parameters as in Fig. 2. Calculations performed using 2.66 GHz Dual-Core Intel Xeon processors and 2 GB RAM. (b) Convergence of response measures for a release site composed of 10 3-state channels using ML_JOR_F_DYN and Monte Carlo (filled and open symbols, respectively). Circles and squares give [illegible] and [illegible] norms of the residual errors, upper pointing triangles give the relative error in the puff/spark Score for Monte Carlo (mean of 50 simulations shown) compared with the Score given by ML_JOR_F_DYN upon convergence. Similarly the lower pointing triangles give the relative error in the probability that all N channels are closed. Parameters as in Fig. 1.

— Model Setup: Approximate Methods —

For one 3-state channel, the state-space $\mathcal{S}$ with a particular partition structure $\mathcal{P}$ is given by $\mathcal{S} = \{C_1, C_2, O_1\}$ and $\mathcal{P} = \{C, O\}$ with $C = \{C_1, C_2\}$, $O = \{O_1\}$. In the case of N 3-state channels, the induced partitioning on the expanded state-space is a mapping from 3^N states to 2^N partitions by [illegible] $\mathcal{S}^N \to p = (p^1 \ldots p^N) \in \mathcal{P}^N$. We can use the *hierarchical Kronecker representation* where the transition matrix Q is decomposed into blocks over partitions $p \neq q$ such that

$$Q^{(N)}[p,p] = \bigoplus_{n=1}^{N} X_n[p^n, p^n] + \sum_{i,j=1}^{N} \bigotimes_{n=1}^{N} X_{ij}^n[p^n, p^n]$$

$$Q^{(N)}[p,q] = \left(\bigotimes_{n=1}^{l-1} I_{[p^n]}\right) X_l[p^l, q^l] \left(\bigotimes_{n=l+1}^{N} I_{[p^n]}\right) + \sum_{i,j=1}^{N} \bigotimes_{n=1}^{N} X_{ij}^n[p^n, q^n]$$

Compositional representation of π corresponding to p is $\pi[p] = \alpha_p \bigotimes_{i=1}^{N} \pi_i^p$ with $\sum_{p \in \mathcal{P}^N} \alpha_p = 1$. The approximate numerical method we consider that leverages this structure is APP_POWER.

— Approximate Methods: Hierarchical Structure —

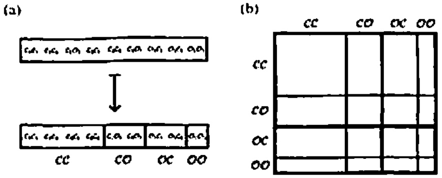

Figure 4 (a) Permutation of states and partition structure for $N = 2$ 3-state channels under the closed/open partitioning strategy $\mathcal{P} = \{C, O\}$ where $C = \{C_1, C_2\}$ and $O = \{O_1\}$. The induced partitioning on $\mathcal{S}^2$ is thus $\mathcal{P}^2 = \{CC, CO, OC, OO\}$ with the states ordered lexicographically in both $\mathcal{S}^2$ and each partition. (b) Block structure of the expanded generator matrix Q when permuted in this manner. The thickness of the lines denotes the hierarchical structure of the partitioning.

— Approximate Methods: Partitioning —

$\|\mathcal{P}\|$	Optimal $\mathcal{P}$ for 3-state model	ϵ	ϵ_{max}	$\rho(3)$	$\rho(12)$
1	$\{C_1C_2O_1\}$	7.64E+0	9.19E-2	3.33E-1	4.77E-5
2	$\{C_1C_2\}\{O_1\}$	5.40E-1	3.53E-3	3.33E+0	1.36E-1
3	$\{C_1\}\{C_2\}\{O_1\}$	4.09E-8	4.38E-9	3.00E+0	1.20E+1

$\|\mathcal{P}\|$	Optimal $\mathcal{P}$ for 6-state model	ϵ	ϵ_{max}	$\rho(3)$	$\rho(5)$
1	$\{C_1C_2R_1R_2R_3O_1\}$	4.04E-1	5.40E-1	8.30E-2	2.86E-5
2	$\{C_1C_2R_1R_2R_3\}\{O_1\}$	3.53E-2	1.36E-2	3.33E-1	3.70E-3
3	$\{C_1C_2\}\{R_1R_2R_3\}\{O_1\}$	9.13E-3	5.50E-3	7.50E-1	4.29E-2
4	$\{C_1\}\{C_2\}\{R_1R_2R_3\}\{O_1\}$	1.57E-4	7.40E-4	1.33E+0	4.49E-1
5	$\{C_1\}\{C_2\}\{R_1R_2\}\{R_3\}\{O_1\}$	5.67E-7	4.12E-7	2.08E+0	2.23E+0
6	$\{C_1\}\{C_2\}\{R_1\}\{R_2\}\{R_3\}\{O_1\}$	4.21E-9	4.16E-9	3.00E+0	8.00E+0

Table 2 Optimal partitioning strategies for APP_POWER listed with their relative errors and memory requirements for both $N = 3$, 3- and 6-state channels with states $\mathcal{S} = \{C_1, C_2, O_1\}$ and $\mathcal{S} = \{C_1, C_2, R_1, R_2, R_3, O_1\}$ respectively (see Fig. 2). The last column also lists relative memory requirements $\rho(N)$ for larger N, where $\rho(N) = Z_A / Z_E$ with $Z_A = N M |\mathcal{P}|^{N-1}$ and $Z_E = M^N$ the memory requirements for the approximate and exact methods respectively. For the 3-state model the optimal $\mathcal{P}$ is the best of 1, 3, 1 possibilities when $|\mathcal{P}| = 1, 2, 3$. For the 6-state model the optimal $\mathcal{P}$ is the best of 1, 31, 90, 65, 15, 1 possibilities when $|\mathcal{P}| = 1, 2, 3, 4, 5, 6$.

— Approximate Methods: Scalability and Error —

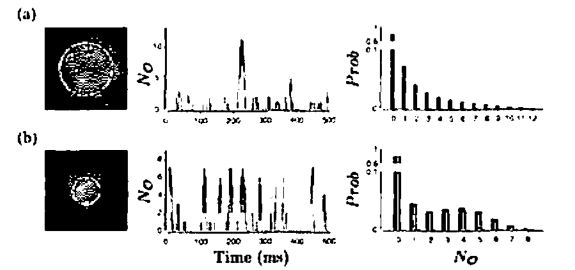

Figure 5 (a) Statistics for a release site composed of 12 3-state channels. Left: Local $[Ca^{2+}]$ near [illegible] ER membrane modeled as in Fig. 1. Middle: Localized Ca^{2+} elevations reminiscent of Ca^{2+} puffs/sparks. Right: Probability distribution of the number of open channels calculated exactly using ML_JOR_F_DYN (black bars) and approximately using APP_POWER with C/O partitioning (white bars). (b) Statistics as in A for 5 6-state channels with black bars denoting ML_JOR_F_DYN and white and grey bars denoting APP_POWER with C/O and C/R/O partitioning, respectively.

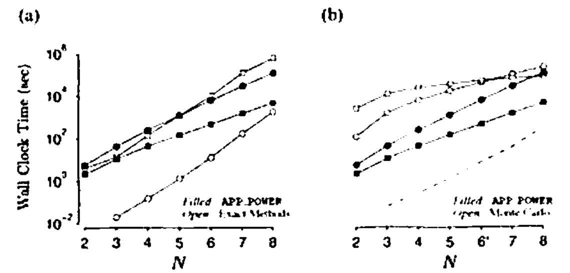

Figure 6 (a) Filled and open symbols show the wall clock time for the 6-state model using approximate and exact methods, respectively. Approximate results are shown for two levels of partitioning (C/O squares and C/R/O circles) with the APP_POWER method. Exact solutions are calculated using the POWER method (squares) and ML_JOR_F_DYN method (circles). (b) Results as in A with open symbols corresponding to Monte Carlo estimates of two coarse response measures: the distribution of the number of open channels (circles) and the distribution of probability across the M states of an arbitrarily selected individual channel (squares). The dashed line shows the projected performance of an approximate multi-level solver that uses ML_JOR_F_DYN rather than POWER as an iterative engine.

— References —

[1] W. Stewart, *Introduction to the numerical solution of Markov chains*, Princeton: Princeton University Press (1994).

[2] V. Nguyen, R. Mathias, and G. D. Smith, *A stochastic automata network descriptor for Markov chain models of instantaneously coupled intracellular Ca^{2+} channels*, Bulletin of Mathematical Biology, 67 (2005), pp 393–432.

[3] H. DeRemigio, M. D. LaMar, P. Kemper, and G. D. Smith, *Markov chain models of coupled calcium channels: Kronecker representations and iterative solution methods*, Physical Biology, 5 (2008).

The authors thank Buchholz and Dayar for sharing their implementation of Nsolve. This material is based upon work supported by the National Science Foundation under Grants No. 0133132 and 0443843.